

The demise of a ‘salt giant’ driven by uplift and thermal dissolution

**Chris Kirkham¹, Claudia Bertoni¹, Joe Cartwright¹, Nadav G. Lensky², Ido Sirota^{2,3},
Karyna Rodriguez⁴ and Neil Hodgson⁴.**

¹ Department of Earth Sciences, University of Oxford, South Parks Road, Oxford, OX1 3 AN,
UK

² Geological Survey of Israel, 32 Yeshayahu Leibowitz Street, Jerusalem 9692100, Israel

³ Institute of Earth Sciences, Hebrew University of Jerusalem, Israel

⁴ Spectrum Geo Ltd. Dukes Court, Duke Street, Woking, Surrey, GU21 5BH, UK

Abstract

The development of giant salt basins and eventual cessation of rapid salt deposition is founded on a delicate balance of salinity and heat fluxes within the water body governed by tectonic, climatic and eustatic change. The onset of salt deposition in such basins is widely accepted to be initiated by basin restriction. However, the processes that lead to the termination of salt deposition are comparatively unclear. Here we use an array of 2D and 3D seismic surveys to reveal that the truncation surface at the top of a thick salt sequence in the Eastern Mediterranean is far more extensive than previously thought. We show that uplift of the salt driven by deformation and thermal dissolution initiated the demise of the ‘salt giant’, even prior to the final dilution and emplacement of brackish Lago Mare and fluvial deposits. Progressive uplift of the salt through the thermocline and into the under-saturated epilimnion led to dissolution. We argue that dissolved salt was recycled and re-precipitation from the hypolimnion in the

deepest sections of the basin contemporaneous with dissolution of halite from the shallower epilimnion. These findings explain how rapid basinwide salt deposition was brought to an end in the Eastern Mediterranean and present a novel process for sculpting the final architecture of a ‘salt giant’.

Keywords: Salt basins; Salt tectonics; Dissolution; Salt recycling; Messinian Salinity Crisis; Eastern Mediterranean

1. Introduction

Marine evaporite sequences covering areas of up to 10^6 km², with thicknesses of several kilometres, are developed in numerous basins worldwide and are indicative of periods of major hydrological change and basin restriction (Warren, 1999; Jackson and Hudec, 2017). The Messinian ‘salt giant’ in the Mediterranean is a rare example of a thick (>1 km) and aerially extensive (ca. 6.7×10^5 km² and ca. 10^6 km³) (Ryan, 1973; Jackson and Hudec, 2017) deep-sea evaporite basin in an immature state of deformation. The evaporite succession in the Eastern Mediterranean is dominated by halite and is partly stratified, characterized by either transparent or strong and laterally continuous internal reflectivity on seismic profiles (Bertoni and Cartwright, 2007; Lofi et al., 2011b) (Fig. 1). The unique continuity of this internal reflectivity provides a rare opportunity for long range correlation of the evaporite stratigraphy of a ‘salt giant’, and allows internal deformation to be defined and mapped regionally and locally (e.g. Feng et al., 2017). The hydrological and basinal dynamics that led to the end of this most dramatic phase of basinwide salt deposition and how it is defined in the geological record have proven elusive.

The upper boundary of the salt sequence in the Eastern Mediterranean, referred to as the Mobile Unit (Lofi et al., 2011b), is widely demarcated by an unconformity, known as the Intra-Messinian Truncation Surface (Gvirtzman et al., 2017) (IMTS; Fig. 1). The extent of intra-Messinian truncation in the Eastern Mediterranean has until now been described primarily in the marginal domains of the Levant Basin (Bertoni and Cartwright, 2007; Lofi et al., 2011b; Feng et al., 2017; Gvirtzman et al., 2017), in the Cyprus Basin and Latakia Basin (Lofi et al., 2011b; Maillard et al., 2011) and recently within a small section of the wider axial domain of the salt basin (Kartveit et al., 2019). Relative sea-level fall (Bertoni and Cartwright, 2007; Kartveit et al., 2019), possibly locally combined with/superimposed to tectonics (Maillard et al., 2011), have been proposed to have led to subaerial exposure and erosion. An alternative model for the IMTS in the marginal Levant Basin was recently proposed by Gvirtzman et al. (2017). In this model, the formation of the truncation surface is not by erosion, but by dissolution as a result of freshening of the water column and the development of a stratified deep water basin (Simon and Meijer, 2017). The dissolution was linked specifically to the uplift of the evaporites along the basin margin, but this interpretation was to some extent conditioned by the limitations of the spatial coverage of the available seismic data used to map the truncation geometry.

In this paper we substantially widen the observational context of this important stratigraphic event towards the end of the Messinian Salinity Crisis (MSC) (Figs. 1b & 2). We utilise a much more extensive database of 2D and 3D seismic than was available for prior studies of the IMTS (Supplementary Fig. 1) to demonstrate considerable truncation (as great as 500 m in thickness) of the top of the Mobile Unit occurred over a much more extensive area of the Eastern Mediterranean than mapped by previous studies (Figs. 1b & 2). The main aim of this paper therefore is to use this database to document the broader context of this important truncation surface and to evaluate current models for its genesis in light of this new mapping. A secondary

aim is to examine the relationship between the important phase of intra-Messinian deformation (*sensu* Bertoni and Cartwright, 2007) and the IMTS. The importance of this question of the origins of the IMTS derives from its significance regarding the events leading to the end of evaporite deposition during the MSC. More widely, this could be considered as a fundamental question about the factors leading to the termination of evaporite depositional systems within a ‘salt giant’.

2. Geological setting

2.1. The Messinian Salinity Crisis and syn-Messinian deformation

The MSC is one of the most dramatic episodes of rapid environmental change in the geological record (Ryan, 2009; Roveri et al., 2014a). The onset of the crisis has been shown to have resulted from the progressive disconnection of the Mediterranean Basin from the Atlantic Ocean (Ryan et al., 1973; Flecker et al., 2015). The resulting negative water balance led to the deposition of thick units of evaporites (Hsu, 1972). The full evaporitic succession was deposited between ~5.97-5.33 Ma (Krijgsman et al., 1999; Manzi et al., 2013; Meilijson et al., 2019). The sea level in the Mediterranean during the MSC is debated (Hsu, 1972), with models ranging from little to no sea level change (Schmalz, 1991; Christeleit et al., 2015; Manzi et al., 2018), to full desiccation (Hsü, 1972; Nesteroff, 1973; Cosentino et al., 2013).

The full evaporitic succession in the Mediterranean, as defined by seismic facies and geometrical relationships, is composed of a Lower Unit, overlain by a Mobile Unit and a Upper Unit the top of which is the top of the MSC units (Lofi et al., 2011b; Lofi, 2018). These three MSC units have only been observed all together in the Western Mediterranean Basin, while

only the Mobile unit and Upper Unit are present in the Eastern Mediterranean (Lofi, 2018; Meilijson et al., 2019).

The chronostratigraphy of MSC has been subdivided into several stages based on correlation of the main lithological units with the astronomical time scale: Stage 1 (5.97-5.6 Ma); Stage 2 (5.6-5.54 Ma); Stage 3.1 (5.54-5.42 Ma); and Stage 3.2 (5.42-5.33 Ma) (Roveri et al., 2014b).

Two contrasting models have been proposed for the relative lengths of time represented by the major lithological units found in marginal and basinal successions (Fig. 3), based on strontium isotope data in DSDP-ODP Messinian cores from around the Mediterranean (Roveri et al., 2014b) and seismic and borehole data from the Levant Basin (Meilijson et al., 2019). In the model proposed by Roveri et al. (2014b) evaporite deposition is absent in the deep basin during Stage 1, with the predominantly halite sequence of the Mobile Unit deposited during Stage 2 and Upper Evaporites (and the Upper Unit) deposited during Stage 3 (Fig. 3), with an increase in terrigenous material defining the onset of Stage 3.2. The model of Meilijson et al. (2019) proposes that the onset of salt (Mobile Unit) deposition in the deep basin was at the beginning of Stage 1 and continued through until the end of Stage 3.1, with the Upper Unit deposited only during Stage 3.2 (Fig. 3). The period over which the exceptionally large volumes of salt that compose the Mobile Unit (Lofi et al., 2011b) were deposited in the deep Mediterranean basins during the MSC therefore ranges from 50-550 ka (Roveri et al., 2014b; Meilijson et al., 2019). The Upper Unit calibrated during DSDP leg 13 at site 376 (Hsü and Montadert, 1978; Kuehn and Hsü, 1978), defines the final stages of evaporite deposition commencing at either 5.54 Ma (Roveri et al., 2014b) or 5.42 Ma (Meilijson et al., 2019). Part of the calibrated Upper Unit is characterized by a change to lower salinity evaporite facies interbedded with clastic sediments and brackish water molluscs and ostracods (Hsü and Montadert, 1978) that signify a period of dilution of the water column. These sediments are also referred to as Lago Mare (Gliozzi et al., 2007; Popescu et al., 2015; Stoica et al., 2016). The deposits immediately above the Mobile

Unit in the South Levant Basin have been calibrated by wells and divided into two units/formations by Druckman et al. (1995) and Gvirtzman et al. (2017): Unit 7 and Afiq Formation, with the evaporites restricted to Unit 7 (Gvirtzman et al., 2017). The upper Messinian fluvial accumulation of the Nahr Menashe also directly overlies large sections of the Mobile Unit in the central-north Levant and Cyprus Basins offshore Lebanon and Syria (Kartveit et al., 2019; Madof et al., 2019).

The study area comprises a large expanse of the present day deeper water region of the Eastern Mediterranean, encompassing the Levant, Herodotus, Antalya, Latakia and Cyprus Basins (Figs. 1b & 2). The Mobile Unit in these basins is typically >1 km, reaching thicknesses >3 km in the deepest basins of the Eastern Mediterranean (Lofi et al., 2011a). Calibration of the Mobile Unit in the South Levant Basin revealed a predominantly halite succession (Feng et al., 2016) with a number of thin layers (metre scale) composed of diatomites interbedded with muddy to sandy clastic sediments (Meilijson et al., 2019). These thin interbedded units correspond with prominent, laterally continuous, high amplitude intra-salt reflections (Feng et al., 2016; Meilijson et al., 2019) that represent valuable markers for deformation in the salt (Cartwright et al., 2012).

Deformation of the Mobile Unit commenced in some parts of the Eastern Mediterranean during the Messinian, and has been attributed in the Levant Basin to some combination of basin tilting through basinal subsidence and marginal uplift (Bertoni and Cartwright, 2007; Gvirtzman et al., 2013). The marginal uplift in the Levant Basin has been attributed to the complex reorganisation of the African and Eurasian Plates and sinistral movement along the Levant Fracture System (Fig. 1b), which has caused the uplift of major onshore structures including Mt Lebanon (Ghalayini et al., 2018), the Judean Mountains (Bar et al., 2016) and the Carmel block (Gvirtzman et al., 2013) since the Mid-Miocene. Uplift of the basin margin and deep basin subsidence during the Messinian led to pronounced westward tilting of the Mobile unit

and its intra-salt layering along the eastern margin of the Levant Basin (Fig. 4), in turn driving basinward salt flow and the syn-Messinian phase of salt deformation in the Levant Basin (Netzeband et al., 2006; Bertoni and Cartwright, 2007; Gvirtzman et al., 2013). Accumulation of the flowing salt in axial domains of the basin resulted in the development of dominantly contractional structures, with wavelengths of a kilometre or so, and thickening and uplift of the Mobile Unit in the deep basin (Bertoni and Cartwright, 2007; Gvirtzman et al., 2013; Feng et al., 2017).

2.2. Seismic stratigraphy of the Mobile Unit in the Eastern Mediterranean

The Mobile Unit in the Eastern Mediterranean is defined by several basinwide key marker horizons (Lofi et al., 2011a). The base of the Mobile Unit is named BES (Bottom Erosional Surface; Fig. 1) (Lofi, 2018) and represents a major, regional erosional unconformity and its correlative conformable surface (Ryan, 1978; Lofi et al., 2011b). The top of the Mobile Unit is referred to variably as Horizon M (Ryan et al., 1973), Top Erosional Surface (Lofi et al., 2011b) (TES) and most recently the Intra-Messinian Truncation Surface (IMTS; Fig. 1) (Gvirtzman et al., 2017). The base and top of the Mobile Unit are demarcated in seismic reflection data as continuous and high amplitude ‘soft’ and ‘hard’ reflections respectively (Figs. 1c & 1d).

The seismic stratigraphy of the Mobile Unit in the Eastern Mediterranean differs considerably between the Levant and Herodotus Basins and Ionian Basin (Fig. 1; Supplementary Fig. 2) (Güneş et al., 2018a; Camerlenghi et al., 2019). In the Levant Basin, the Mobile Unit comprises several high amplitude and laterally correlatable intra-salt reflections (ME20 – ME60) that alternate with seismically transparent layers, forming a recognisably layered succession consisting of six units (ME-I – ME-VI) (Figs. 1 & 4) (Bertoni and Cartwright, 2007; Lofi et al., 2011a; Lofi et al., 2011b). Other nomenclature including Unit 1 - Unit 6 (Gvirtzman et al.,

2017), and ME1 – ME4 (ME – Messinian Evaporites) and MC1 – MC2 (MC – Messinian
Clastics) (Feng et al., 2016), are utilized in other publications for the same sequence (Fig. 3).
In the Herodotus Basin, there are only two clear seismically defined units that comprise the
Mobile Unit, a lower highly reflective unit (MLM – Messinian Lower Megasequence) and a
transparent upper unit (MUM – Messinian Upper Megasequence; Figs. 1a, 1c & 3) (Gorini et
al., 2015). The entire succession in the Herodotus Basin is uncalibrated, but the MLM has been
linked to continued clastic supply from the Nile Messinian cone (Gorini et al., 2015). The
junction between these two contrasting seismic stratigraphic packages is observed southeast of
the Eratosthenes Block. Here seismic profiles show that ME20 – ME60 transition into the
MLM, with ME60 demarcating the top of the MLM (Figs. 1a; Supplementary Fig. 2). ME-VI
represents the eastern extent of the MUM, which exhibits a regional wedge shape geometry
that increases in thickness toward the Herodotus Basin and thins towards the Levant Basin,
where beyond its regional pinch out it is only preserved in synclinal axes (Figs. 1a, 4 & 5).

3. Data and methodology

The seismic data available for this study consists of several regional 2D surveys and two 3D
seismic surveys (Supplementary Fig. 1). The 3D seismic data used in the study was acquired
in 2012 by Spectrum with a bin spacing of 12.5 m which results in an effective lateral resolution
of 25 m in the interval of interest. Dominant frequency for all the surveys is 50Hz and 30Hz in
the post-Messinian interval and Mobile Unit, respectively for which average P wave velocities
of 2,000 m/s and 4,200 m/s yield vertical resolutions of 10 m and 35 m (Brown, 2011). Velocity
values are calculated from petrophysical data from exploration wells in the Levant Basin (Feng
et al., 2016) and were used to depth convert the Mobile Unit and post-Messinian succession

(Supplementary Fig. 3). The 2D and 3D seismic data are pre-stack time migrated, processed to a zero phase wavelet, and displayed with a polarity such that acoustically hard reflections (increase of acoustic impedance downwards) are displayed on the profile as positive amplitudes.

Seismic interpretation was performed using Schlumberger's Petrel 3D seismic software platform. Horizons were picked manually along the 2D seismic lines and interpolated to produce gridded surfaces (Brown, 2011). Horizons interpreted within the 3D seismic volume were manually picked in grids of 100 m spacing and autocorrelated to produce continuous surfaces. RMS amplitude volumes were computed, extracted along the mapped IMTS horizon and interpreted to identify features related to subcropping intra-salt reflections. For reasons pertaining to confidentiality the exact location and full two-way time (TWT) of the seismic profiles could not be displayed, however, the general region that they are taken from is highlighted (Fig. 2).

4. Results

The IMTS is interpretable on seismic profiles wherever underlying intra-salt reflections within the Mobile Unit have been deformed or tilted during the Late Messinian into a discordant relationship with the overlying latest Messinian and Pliocene sediments (Figs. 4-6; Supplementary Fig. 4a). Its full extent (Fig. 1b) is established by regional mapping of discordant and truncated intra-salt reflections using 2D and 3D seismic data (Figs. 2, 4 & 5). This deformation is contractional in geometry over >60% of the basin, with well-developed symmetric to asymmetric folds with amplitudes of 100-600 m, open hinges, and inter-limb angles ranging from 40 to 160° (Figs. 4b & 5). In contrast to previous studies our mapping

shows that the IMTS forms a vast basinwide unconformity surface that encompasses marginal and axial domains of the various sub-basins (Figs. 1a, 1b & 2). It extends across the Latakia Basin, Cyprus Basin, Levant Basin, south of the Eratosthenes and further westward as far as the Herodotus Basin and north of the Florence Rise in the Antalya Basin.

The IMTS is mapped throughout the area of seismic data coverage with lower and upper confidence levels, respectively as 1 or $1.1 \times 10^5 \text{ km}^2$. Upper confidence and lower confidence values are computed based on the distribution of clear truncations (Figs. 4 & 5) and others that are less definitive (Supplementary Fig. 4a). These more uncertain truncations are distributed in the Herodotus Basin, where 2D seismic coverage is sparser (Supplementary Fig. 1), the MUM is thicker (Fig. 1a) and there has been significant post-Messinian deformation of the Mobile Unit. Where the Mobile Unit is undeformed, it proved impossible to recognise any unconformity in the the concordant geometry of the Mobile Unit and overlying Pliocene reflections. The removal of salt at the top of the Mobile Unit cannot be excluded in these areas, but cannot be directly inferred from the seismic data alone.

The IMTS is remarkably continuous and very smooth over the full extent of its huge area, with only limited palaeo-relief of <50 m developed locally (Fig. 6). No incised valleys or any other incisional erosional features have been mapped anywhere at the IMTS around the basin. Relict topography is only evident where high amplitude seismic reflections subcrop the IMTS, consistent with lithological changes calibrated by boreholes (Feng et al., 2016) (Fig. 6). These subcrops are displayed as linear to irregularly distributed regions of increased amplitude in RMS amplitude maps with rugose geometry in planform (Fig. 6).

Subcrops of truncated intra-salt folds are distributed extensively within the central Levant Basin and Herodotus Basin (Figs. 2, 4 & 5). Reconstruction of the truncated geometries of these folds allowed the minimum values of truncated removal to be calculated for many of the most prominent folds and these values range from 180 m to 760 m (Fig. 2).

249 Along the eastern margin of the Levant Basin, the IMTS is characterized by a continuous
250 subcrop belt of tilted and truncated intra-salt reflections (ME20-ME60) (Figs. 2 & 4a). Their
251 subcrop geometry strikes parallel to the basin margin continuously over a distance 400 km
252 along strike (Figs. 2 & 4a). At the eastern limit of this marginal truncation, the entire Messinian
253 has been removed (Fig. 4a), and thus involves removal of at least 1000 m of predominantly
254 salt.

255 Two contrasting ‘uplifting’ processes are therefore evident when considering the truncation
256 geometries at the IMTS. Firstly, the Intra-Messinian contractional deformation thickened and
257 uplifted the Mobile Unit in the basin axes resulting in truncation of anticlinal crests and of the
258 intra-salt layers within. Secondly, there was substantial tilting and uplift, with a tilt direction
259 generally orthogonal to the eastern margins of the Levant Basin and truncation parallel to the
260 basin margin (Figs. 1a & 4).

261 Taken together, these two distinct types of truncation geometry observed over vast areas
262 suggest that the marginal tilting is unlikely to have been a local isostatic effect produced by
263 earlier basin loading by evaporites (Govers et al., 2009). Instead it seems more plausible that
264 regional tectonics played a role in this combined deformation (Maillard et al., 2011). Previous
265 suggestions of a salt tectonic detachment horizon and shearing at the top of the Mobile Unit
266 (Cartwright et al., 2012), related to deformation during the Pliocene to Recent, cannot account
267 for the thickness of salt removed from the top of the Mobile Unit and is not compatible with
268 the large areal extent of truncated Messinian (Figs. 2 & 5), encompassing both marginal and
269 axial domains (Fig. 4).

270 The IMTS does not extend into two regions over which we have seismic data coverage in the
271 Eastern Mediterranean: the deeper segments of the northern Herodotus Basin and the Cyprus
272 Trench, over an area of $1.1 \times 10^4 \text{ km}^2$ (Fig. 1b). No discordant geometries, truncations of intra-
273 salt reflections or any other obvious evidence of removal of section are interpretable wherever

the IMTS is not mappable (Supplementary Fig. 4b). These regions are characterised by a deepening of the Bottom Erosional Surface (BES) relative to those areas where the IMTS is recognised and an increase in thickness of the Mobile Unit from a regional value of 1.4 to 2 km to over 5 km (Supplementary Fig. 3).

Thrusting at the Florence Rise due to the collision of Africa and Eurasia during the pre-Messinian Miocene formed a depocentre south of the prominent ridge prior to the MSC and salt deposition (Güneş et al., 2018b). Continued convergence during the Pliocene to Recent led to tectonic thickening of the original depositional salt thickness within this depocenter to the present day 5 km (Supplementary Fig. 3). The post-Messinian shortening was calculated as 13 +/- 1.5 km using standard line length balancing techniques (Dahlstrom, 1969), yielding 500 m (+/-100 m) of tectonic thickening of the salt. The Mobile Unit prior to tectonic thickening was, therefore, probably in excess of 4.4 km, demonstrating the presence of a large depocentre south of the Florence Rise (northern Herodotus Basin) during the MSC and the accumulation of an exceptional thickness of salt.

5. Discussion

5.1. Subaerial vs subaqueous origin of the IMTS

Two competing models for the origin of the IMTS are (1) subaerial erosion linked with relative sea-level fall (Bertoni and Cartwright, 2007; Kartveit et al., 2019) that is locally in parts of the basin combined with/superimposed to tectonics (Maillard et al., 2011), or (2) subaqueous dissolution in a stratified water column in a deepwater setting where the tilted basinal evaporites were uplifted above a chemocline along the basin margin (Gvirtzman et al., 2017).

298 The much more laterally extensive region of truncation implied by the new mapping of the
299 IMTS (Figs. 1b & 2) strongly favours a subaqueous dissolution model. The smooth geometry
300 of this surface over its vast areal extent is incompatible with fluvial erosion, as is the absence
301 of any significant large scale incisional relief (Druckman et al., 1995; Cantón et al., 2001;
302 Martinez et al., 2004). Fluvial gradients would have had to be less than c. 1:500 over the region
303 of erosion, simply from the 100s km dimensions of the eroded region with respect to fluvial
304 entry points at the basin margins, and it is difficult to see how fluvial systems under such low
305 gradients could have avulsed efficiently so as to result in the final, low relief planation surface.
306 Furthermore, it is unlikely that the necessary water depths of 10-20 m for vigorous wave
307 erosion (Bache, 2012) could have been maintained over the $1.0\text{-}1.1 \times 10^5 \text{ km}^2$ area of the IMTS
308 through the period when the truncation developed. It is also unlikely that in the confined basin
309 setting east of the major central Mediterranean Sicily Channel Sill (Camerlenghi et al., 2019),
310 that the limited fetch would have produced sufficient wave energy for any significant truncation
311 to take place.

312 The subaqueous dissolution model proposed by Gvirtzman et al. (2017) instead provides an
313 efficient means to remove large quantities of evaporitic sediments over the large area of
314 truncation without producing more localised focused erosional features. Subaqueous
315 dissolution can remove salt layers at rates of up to 1 cm/a when exposed to oceanic salinities
316 of 36.3 g/L (Pilcher and Blumstein, 2007), and higher rates of up to 10 cm/a have been
317 recorded in the Dead Sea (Sirota et al., 2017) where dissolution is thermally controlled.

318 As a restricted basin during the MSC the only outlet from the Mediterranean for the salt
319 dissolved in the Eastern Mediterranean would have been beyond the Western Mediterranean
320 and through the connection with the Atlantic via the Gibraltar Strait (Flecker et al., 2015). The
321 seismic stratigraphy of the Messinian Evaporites in the Western Mediterranean is composed of
322 a Lower Unit, Mobile Unit and Upper Unit (Lofi et al., 2011b). This contrast in seismic

323 stratigraphy and expression compared to the Messinian Evaporites in the Eastern
324 Mediterranean has been attributed to separation of the two basins during the MSC by the
325 regional Sicily Channel Sill (Blanc, 2000; Roveri et al., 2014b; Camerlenghi et al., 2019).
326 Dammed by the buttress of the Sicily Sill it is conceivable that it was not possible for any
327 hypersaline waters to outflow from the Eastern Mediterranean, implying that the large volumes
328 of dissolved salt may have been trapped and remained in the Eastern Mediterranean Basin.
329 What would have been the fate of the dissolved salt? The wedge geometry (Fig. 1a) and
330 substantial thickening of the MUM/ME-VI toward regions where the IMTS is absent (Figs. 1b;
331 Supplementary Figs. 3 & 4b) such as south of the Florence Rise, implies that no widespread
332 and continuous dissolution took place in these areas. It is conceivable that in these deepest
333 sections of the basin salt deposition continued during the period that truncation was occurring
334 elsewhere in the basin, in order to achieve the anomalous thicknesses observed in combination
335 with no evidence of truncation (Supplementary Figs. 3 & 4b). One possible explanation for the
336 fate of the dissolved salt, that would also explain the observed geometrical configuration of the
337 MUM, is that it was re-precipitated from the water column as recycled salt, analogous to salt
338 recycling described in the presently forming Dead Sea salt basin (Sirota et al., 2017; Sirota et
339 al., 2018). Primary and recycled salt would be indistinguishable in seismic reflection data
340 because there is little compositional difference to produce an acoustic impedance contrast. The
341 primary and recycled salt will be composed of a reflection-free or opaque seismic facies typical
342 of pure halite, therefore, it is not possible to identify recycled salt using seismic data alone.
343 However, cores from DSDP Site 376 (Fig. 2) documented the presence of halite in this area,
344 characterised by low bromine content, which is indicative of salt recycling (Hsü and Montadert,
345 1978; Kuehn and Hsü, 1978; Lugli et al., 1999). The “sink” of recycled salt could also be
346 located west of where the IMTS is interpreted here, or even outside of the study area in the
347 Ionian Basin where there Mobile Unit is also particularly thick (Camerlenghi et al., 2019).

Some form of stratification is to be expected and is a pre-requisite for subaqueous dissolution in a hypersaline salt precipitating water column that is restricted from global oceans (Simon and Meijer, 2017). The lateral extent of the IMTS should therefore simply correlate with the geometry of the stratified water body. The key question is therefore how to explain the development of this stratification, and can it account for the dissolution as well as the potential for recycling?

5.2. Processes governing the dissolution and recycling of the Messinian salt

An under-saturated upper water column (epilimnion) is a prerequisite for the subaqueous dissolution described here, and can be achieved either by dilution or by heating of the water column. The dilution model requires a significant and persistent flux of marine or fresher water into the basin, forming a diluted upper layer that is divided from the underlying salt saturated hypolimnion by a chemocline (Gvirtzman et al., 2017). This model is associated with a positive water balance and thus does not allow for the continuation of salt deposition after dilution, even in the non-diluted hypolimnion (lower water column) (Hsu, 1972; Lensky et al., 2005). Dissolution in the epilimnion results in the formation of a hypersaline brine over the salt layers. This brine is denser than the overlying diluted epilimnion, thus is gravitationally stable, and is nearly halite-saturated, therefore reducing the efficiency of further salt dissolution. Moreover, this type of stratification results in the upward transport of dissolved salt ions along the salinity gradient, implying that a transfer of dissolved salt to a saltier underlying hypolimnion is unlikely (Neev et al., 1967; Stiller et al., 1997). The density of the diluted epilimnion, after achieving full saturation, would reach ~1.19 g/cc, which is still lighter than the more evolved hypolimnetic saturated brine due to the load of other ions (e.g. Mg, Ca, K; densities of >1.24 g/cc measured in the Dead Sea (Sirota et al., 2016)). Hence, a density driven transfer of salt into the depocenter across the chemocline is unlikely in the diluted upper water column model.

A chemoclinally diluted water column is, therefore, incapable of permitting the required fluxes of salt between the epilimnion and hypolimnion, in order for salt recycling and continued salt deposition in the deep basin contemporaneous to dissolution across shallower regions. New insights for thermal dissolution and salt recycling are provided by detailed recent studies of the present day Dead Sea (Sirota et al., 2017), representing the closest and probably only modern analogue of an actively forming deep salt basin. The lake is governed by a continuous negative water budget, which drives salt deposition (Lensky et al., 2005). Salt dissolution occurs during warmer seasons in the basin when net evaporation is at its highest rates (Sirota et al., 2016). The influence that temperature and heating of the upper water column has on saturation during warmer summer periods overcomes the increasing salinity, resulting in under-saturation of the epilimnetic brine (Sirota et al., 2016). This allows a flux of dissolved salt from the warmer and saltier epilimnion to the less salty and colder hypolimnion, via double diffusion salt fingering across the thermocline (Stern, 1960; Arnon et al., 2016; Ouillon et al., 2019). The result is salt super-saturation in the hypolimnion coeval with salt under-saturation in the epilimnion. Thermal stratification in the restricted Eastern Mediterranean analogous to the Dead Sea was also recently proposed by (Meilijson et al., 2019) and is certain to have occurred due to seasonal warming of surface water, typical of mid latitude and arid regions. In contrast to a dilution chemocline model, this process would permit the dissolution of salt over a vast region of the basin contemporaneous with salt recycling and continued precipitation at the hypolimnetic basin floor (Sirota et al., 2017; Sirota et al., 2018).

5.3. Model for uplift and thermally driven dissolution of the Messinian Salt Giant

Based on the analogy with the Dead Sea evaporite depositional system, we suggest a simple two step model for dissolution and salt recycling, leading to basinwide cessation of salt deposition in the Eastern Mediterranean (Fig. 7). Firstly, the Mobile Unit sequences of MEI-

398 MEVI in the Levant Basin and the MLM and an unknown height of the MUM in the Herodotus
399 Basin were deposited uniformly and synchronously (Fig. 7a). Deposition of this predominantly
400 halite sequence could have taken place at a range of water depths, none less than a few 100 m
401 (Fig. 7a). At water depths less than 100 m the epilimnion would have come into contact with
402 the Mobile Unit in the deep basin during warmer seasons leading to dissolution as opposed to
403 deposition, by analogy with the Dead Sea (Sirota et al., 2016).

404 Secondly, a reduction in water column height in the Eastern Mediterranean Basin (Fig. 7b), to
405 depths ranging from 10s to a few 100s of meters, must have taken place to lower the position
406 of the thermocline during warmer summer periods. This could be achieved by reducing water
407 inflow into the basin or increasing evaporation during a period of warming (Blanc, 2000; Simon
408 and Meijer, 2017). The lowest relative sea level at the Atlantic side of the Gibraltar Strait (Rif-
409 Betic corridors before the MSC) is measured at 5.57 Ma and would have reduced the inflow of
410 Atlantic waters at the ‘Gibraltar’ Strait during Stage 2, prior to Stage 3 deposition (Ohneiser et
411 al., 2015). The palaeo climate in the Mediterranean during Stage 2 and Stage 3 underwent a
412 period (5.6-5.3 Ma) of transition from colder and humid to warmer and arid, recorded using
413 biomarkers of C₂₉ and C₃₁ n-alkanes and C₂₇ and C₃₈ long chain alkenones in samples from the
414 Messinian sequence (Vasiliev et al., 2017), which will have increased evaporation from the
415 basin. The relative sea level fall caused the summit of the Eratosthenes Block to be exposed
416 above the water column and subjected to subaerial weathering processes (Major and Ryan,
417 1999; Van Simaeys et al., 2019). Syn-Messinian uplift and tilting of the Levant margin and
418 deep basin subsidence (Gvirtzman et al., 2013; Bar et al., 2016; Ghalayini et al., 2018),
419 combined with the development of contractional structures and thickening of the salt
420 (Netzeband et al., 2006; Bertoni and Cartwright, 2007; Gvirtzman et al., 2013; Feng et al.,
421 2017), uplifted the Mobile Unit through the thermocline in both marginal and axial domains
422 (Fig. 7b). The uplifted salt was exposed to under-saturated water in the epilimnion during

summer periods, leading to dissolution (Fig. 7c). The rate of uplift must have exceeded the flow rate of the salt, while the dissolution rate must have exceeded the uplift rate in order to produce such well-preserved truncated folds in salt and a smooth IMTS. The cumulative effect of uplift of the Mobile Unit combined with this seasonal dissolution phenomenon was significant over a geological time scale, giving rise to a vast truncation surface over which 100 s of meters of salt thickness were dissolved.

The deepest regions of the basin, including large parts of the northern Herodotus Basin, remained within the hypolimnion and did not experience dissolution (Figs. 1b & 7b). The basinward limit of the IMTS (Fig. 1b) indicates the lowest level of the thermocline during the period of dissolution. The dissolved salt was transferred to the hypolimnion via double diffusion salt fingering, where it was recycled and re-deposited together with primary salt deposition, during continued salt precipitation at the hypolimnetic seafloor contemporaneous to dissolution in the epilimnion (Fig. 7c). Low bromine contents observed in halite samples from DSDP Site 376 located on the Florence Rise (Fig. 2) support this model of salt recycling in the deeper basin (Hsü and Montadert, 1978; Kuehn and Hsü, 1978; Lugli et al., 1999). A further sea level fall and subaerial exposure of large parts of the basin during stage 3 is invoked by the development of the fluvial Nahr Menashe system (Madof et al., 2019) that overlies the IMTS. The stratigraphic position of the IMTS implies that the genesis of the IMTS pre-dates the further sea level fall and development of this late Messinian fluvial system. While it is not possible to precisely date the end of the dissolution and recycling phase, recent drilling results within the deeper part of the Levant Basin show that the units deposited directly above the IMTS (Gvirtzman et al., 2017) correspond to the Upper Evaporites assemblage marking Stage 3.1 (Roveri et al., 2014b; Gvirtzman et al., 2017) or Stage 3.2 (Meilijson et al., 2019) of the MSC. The dissolution and recycling episode and formation of ME-VI and its laterally equivalent MUM hence took place either prior to the start of Stage 3 deposition dated at 5.54

Ma within the onshore realm (Roveri et al., 2014b), or prior to Stage 3.2 dated at 5.42 Ma based on the recent model proposed by Meilijson et al. (2019). Despite uncertainty in precise timing, both existing models agree that the truncation and recycling took place prior to the Zanclean flood and re-establishment of a full connection to the Atlantic at 5.33 Ma.

This study demonstrates that a combination of uplift and thermally driven dissolution can terminate salt deposition on a basin scale. It is plausible that due to the buttress of the Sicily Channel Sill and processes analogous to those observed in the Dead Sea that dissolved salt was recycled and re-precipitated in the deep basin, contemporaneous with more proximal shallow water dissolution. This process implies that the end of salt deposition within the Eastern Mediterranean was not synchronous across the entire basin, with the deepest parts only terminating with Stage 3 freshwater dilution and the complete switch off of salt deposition. With regards to the rest of the Mediterranean, the salt stratigraphy of the Western Mediterranean contrasts significantly with that of the Eastern Mediterranean (Lofi et al., 2011a; Lofi et al., 2011b) and it is at present unclear how salt deposition ended in the Western Mediterranean or even if the timing of the termination is the same between the basins of the Mediterranean, with events likely diachronous. The fundamental requirements of tectonic uplift of salt and thermal stratification of the water column are not considered likely to be exclusive to the Eastern Mediterranean simply because at water depths up to few 100s of meters, thermally controlled dissolution plays a crucial role in the balance between deposition and dissolution. Hence this process will likely have sculpted the final architecture of other ‘salt giants’.

6. Conclusions

1. A broad seismic database reveals the basinwide extent of a truncation surface (IMTS) at the top of the salt (Mobile Unit) that formed during the Messinian Salinity Crisis in the Eastern Mediterranean.
2. The truncation surface was formed by subaqueous dissolution within a seasonally/thermally controlled stratified water column.
3. The truncation surface was the result of a major phase of syn-Messinian deformation that progressively uplifted the salt through the thermocline and into the thermally undersaturated epilimnion where it was dissolved.
4. The dissolved salt was transferred to the hypolimnion via double diffusion salt fingering, where it was recycled and re-deposited contemporaneous with dissolution in the epilimnion. The result is anomalously thick salt deposits (> 5 km) in the deepest regions of the basin, which represent the “sink” of recycled salt.
5. The end of salt deposition was diachronous in the Eastern Mediterranean, with salt deposition persisting in the deepest parts of the basin while the Mobile unit was dissolved proximally, until Stage 3 freshwater dilution and the complete end of salt deposition.
6. The process of terminating salt deposition via uplift and thermally driven dissolution has important implication for the terminal stages of salt deposition in large salt basins globally and is likely to have played an important role in sculpting their final architecture.

Acknowledgements

We would like to thank the editor An Yin and the anonymous reviewer for their insightful and constructive comments that helped greatly in improving the manuscript. Thank you to TGS (previously Spectrum) for provision of the seismic reflection data and we acknowledge

Schlumberger for provision of the seismic interpretation software used. NGL was supported by the Israel Science Foundation, grant # ISF 1471/18 and USA – Israel Binational Science Foundation, grant # BSF 2018/035.

References

- Arnon, A., Selker, J. & Lensky, N. 2016. Thermohaline stratification and double diffusion diapycnal fluxes in the hypersaline Dead Sea. *Limnology and Oceanography*, 61, 1214-1231.
- Bache, F. 2012. A two step process for the reflooding of the Mediterranean after the Messinian salinity crisis. *Basin Research*, 24, 125-153.
- Bar, O., Zilberman, E., Feinstein, S., Calvo, R. & Gvirtzman, Z. 2016. The uplift history of the Arabian Plateau as inferred from geomorphologic analysis of its northwestern edge. *Tectonophysics*, 671, 9-23.
- Bertoni, C. & Cartwright, J. 2007. Major erosion at the end of the Messinian Salinity Crisis: evidence from the Levant Basin, Eastern Mediterranean. *Basin Research*, 19, 1-18.
- Blanc, P.-L. 2000. Of sills and straits: a quantitative assessment of the Messinian Salinity Crisis. *Deep Sea Research Part I: Oceanographic Research Papers*, 47, 1429-1460.
- Brown, A. R. 2011. *Interpretation of three-dimensional seismic data*, Society of Exploration Geophysicists and American Association of Petroleum Geologists.
- Camerlenghi, A., Del Ben, A., Hübscher, C., Forlin, E., Geletti, R., Brancatelli, G., Micallef, A., Saule, M. & Facchin, L. 2019. Seismic markers of the Messinian salinity crisis in the deep Ionian Basin. *Basin Research*.
- Cantón, Y., Domingo, F., Solé-Benet, A. & Puigdefábregas, J. 2001. Hydrological and erosion response of a badlands system in semiarid SE Spain. *Journal of Hydrology*, 252, 65-84.

522 Cartwright, J., Jackson, M., Dooley, T. & Higgins, S. 2012. Strain partitioning in gravity-driven
523 shortening of a thick, multilayered evaporite sequence. *Geological Society, London, Special*
524 *Publications*, 363, 449-470.

525 Christeleit, E. C., Brandon, M. T. & Zhuang, G. 2015. Evidence for deep-water deposition of abyssal
526 Mediterranean evaporites during the Messinian salinity crisis. *Earth and Planetary Science*
527 *Letters*, 427, 226-235.

528 Cosentino, D., Buchwaldt, R., Sampalmieri, G., Iadanza, A., Cipollari, P., Schildgen, T. F., Hinnov, L. A.,
529 Ramezani, J. & Bowring, S. A. 2013. Refining the Mediterranean “Messinian gap” with high-
530 precision U-Pb zircon geochronology, central and northern Italy. *Geology*, 41, 323-326.

531 Dahlstrom, C. 1969. Balanced cross sections. *Canadian Journal of Earth Sciences*, 6, 743-757.

532 Druckman, Y., Buchbinder, B., Martinotti, G., Tov, R. S. & Aharon, P. 1995. The buried Afik Canyon
533 (eastern Mediterranean, Israel): a case study of a Tertiary submarine canyon exposed in Late
534 Messinian times. *Marine Geology*, 123, 167-185.

535 Feng, Y. E., Steinberg, J. & Reshef, M. 2017. Intra-salt deformation: Implications for the evolution of
536 the Messinian evaporites in the Levant Basin, eastern Mediterranean. *Marine and Petroleum*
537 *Geology*, 88, 251-267.

538 Feng, Y. E., Yankelzon, A., Steinberg, J. & Reshef, M. 2016. Lithology and characteristics of the
539 Messinian evaporite sequence of the deep Levant Basin, eastern Mediterranean. *Marine*
540 *Geology*, 376, 118-131.

541 Flecker, R., Krijgsman, W., Capella, W., De Castro Martíns, C., Dmitrieva, E., Mayser, J. P., Marzocchi,
542 A., Modestou, S., Ochoa, D. & Simon, D. 2015. Evolution of the Late Miocene
543 Mediterranean–Atlantic gateways and their impact on regional and global environmental
544 change. Elsevier.

545 Ghalayini, R., Nader, F., Bou Daher, S., Hawie, N. & Chbat, W. 2018. Petroleum systems of Lebanon:
546 An update and review. *Journal of Petroleum Geology*, 41, 189-214.

547 Gliozzi, E., Ceci, M. E., Grossi, F. & Ligios, S. 2007. Paratethyan ostracod immigrants in Italy during
 548 the Late Miocene. *Geobios*, 40, 325-337.

549 Gorini, C., Montadert, L. & Rabineau, M. 2015. New imaging of the salinity crisis: Dual Messinian
 550 lowstand megasequences recorded in the deep basin of both the eastern and western
 551 Mediterranean. *Marine and Petroleum Geology*, 66, 278-294.

552 Govers, R., Meijer, P. & Krijgsman, W. 2009. Regional isostatic response to Messinian Salinity Crisis
 553 events. *Tectonophysics*, 463, 109-129.

554 Güneş, P., Aksu, A. & Hall, J. 2018a. Internal seismic stratigraphy of the Messinian evaporites across
 555 the northern sector of the eastern Mediterranean Sea. *Marine and Petroleum Geology*, 91,
 556 297-320.

557 Güneş, P., Aksu, A. & Hall, J. 2018b. Structural framework and deformation history of the western
 558 Cyprus Arc. *Tectonophysics*, 744, 438-457.

559 Gvirtzman, Z., Manzi, V., Calvo, R., Gavrieli, I., Gennari, R., Lugli, S., Reghizzi, M. & Roveri, M. 2017.
 560 Intra-Messinian truncation surface in the Levant Basin explained by subaqueous dissolution.
 561 *Geology*, 45, 915-918.

562 Gvirtzman, Z., Reshef, M., Buch-Leviatan, O. & Ben-Avraham, Z. 2013. Intense salt deformation in the
 563 Levant Basin in the middle of the Messinian Salinity Crisis. *Earth and Planetary Science*
 564 *Letters*, 379, 108-119.

565 Hsu, K. 1972. Origin of saline giants: a critical review after the discovery of the Mediterranean
 566 evaporite. *Earth-Science Reviews*, 8, 371-396.

567 Hsü, K. & Montadert, L. 1978. Sites 375 and 376: Florence Rise. *Initial Reports of the Deep-Sea*
 568 *Drilling Project. Edited by KJ Hsü and L. Montadert*, 42, 219-304.

569 Hsü, K. J. 1972. When the Mediterranean dried up. *Scientific American*, 227, 26-39.

570 Jackson, M. P. & Hudec, M. R. 2017. *Salt tectonics: Principles and practice*, Cambridge University
 571 Press.

572 Kartveit, K. H., Ulsund, H. B. & Johansen, S. E. 2019. Evidence of sea level drawdown at the end of
573 the Messinian Salinity Crisis and seismic investigation of the Nahr Menashe Unit in the
574 northern Levant Basin, offshore Lebanon. *Basin Research*.

575 Krijgsman, W., Hilgen, F., Raffi, I., Sierro, F. J. & Wilson, D. 1999. Chronology, causes and progression
576 of the Messinian salinity crisis. *Nature*, 400, 652.

577 Kuehn, R. & Hsü, K. 1978. Chemistry of halite and potash salt cores, DSDP Sites 374 and 376, Leg
578 42A, Mediterranean Sea. *Initial Reports of the Deep Sea Drilling Project*, 42, 613-619.

579 Lensky, N., Dvorkin, Y., Lyakhovsky, V., Gertman, I. & Gavrieli, I. 2005. Water, salt, and energy
580 balances of the Dead Sea. *Water Resources Research*, 41.

581 Lofi, J. 2018. Seismic Atlas of the Messinian Salinity Crisis markers in the Mediterranean Sea-Volume
582 2.

583 Lofi, J., Déverchère, J., Gaullier, V., Gillet, H., Gorini, C., Guennoc, P., Loncke, L., Maillard, A., Sage, F.
584 & Thinon, I. 2011a. *Seismic atlas of the Messinian Salinity Crisis markers in the*
585 *Mediterranean and Black Seas*, Société Géologique de France.

586 Lofi, J., Sage, F., Déverchère, J., Loncke, L., Maillard, A., Gaullier, V., Thinon, I., Gillet, H., Guennoc, P.
587 & Gorini, C. 2011b. Refining our knowledge of the Messinian salinity crisis records in the
588 offshore domain through multi-site seismic analysis. *Bulletin de la Société géologique de*
589 *France*, 182, 163-180.

590 Lugli, S., Schreiber, B. C. & Triberti, B. 1999. Giant polygons in the Realmonte Mine (Agrigento,
591 Sicily); evidence for the desiccation of a Messinian halite basin. *Journal of Sedimentary*
592 *Research*, 69, 764-771.

593 Madof, A. S., Bertoni, C. & Lofi, J. 2019. Discovery of vast fluvial deposits provides evidence for
594 drawdown during the late Miocene Messinian salinity crisis. *Geology*, 47, 171-174.

595 Maillard, A., Hübscher, C., Benkhelil, J. & Tahchi, E. 2011. Deformed Messinian markers in the Cyprus
596 Arc: tectonic and/or Messinian Salinity Crisis indicators? *Basin Research*, 23, 146-170.

597 Major, C. & Ryan, W. B. 1999. Eratosthenes seamount: record of late Miocene sea-level changes and
 598 facies related to the Messinian Salinity Crisis. *Memorie della Società Geologica Italiana*, 54,
 599 47-59.

600 Manzi, V., Gennari, R., Hilgen, F., Krijgsman, W., Lugli, S., Roveri, M. & Sierro, F. J. 2013. Age
 601 refinement of the Messinian salinity crisis onset in the Mediterranean. *Terra Nova*, 25, 315-
 602 322.

603 Manzi, V., Gennari, R., Lugli, S., Persico, D., Reghizzi, M., Roveri, M., Schreiber, B. C., Calvo, R.,
 604 Gavrieli, I. & Gvirtzman, Z. 2018. The onset of the Messinian salinity crisis in the deep
 605 Eastern Mediterranean basin. *Terra Nova*, 30, 189-198.

606 Martinez, J. F., Cartwright, J. A., Burgess, P. M. & Bravo, J. V. 2004. 3D seismic interpretation of the
 607 Messinian Unconformity in the Valencia Basin, Spain. *Geological Society, London, Memoirs*,
 608 29, 91-100.

609 Meilijson, A., Hilgen, F., Sepúlveda, J., Steinberg, J., Fairbank, V., Flecker, R., Waldmann, N. D.,
 610 Spaulding, S. A., Bialik, O. M. & Boudinot, F. G. 2019. Chronology with a pinch of salt:
 611 Integrated stratigraphy of Messinian evaporites in the deep Eastern Mediterranean reveals
 612 long-lasting halite deposition during Atlantic connectivity. *Earth-Science Reviews*.

613 Neev, D., Goldschmidt, M., Ettinger, M. I., Arad, A., Buchbinder, B., Emery, K. O., Hamaoui, M. &
 614 Langozki, Y. 1967. *The Dead Sea: depositional processes and environments of evaporites*,
 615 State of Israel, Ministry of Development, Geological Survey.

616 Nesteroff, W. D. 1973. Un modèle pour les évaporites messiniennes en Méditerranée: Des bassins
 617 peu profonds avec dépôts d'évaporites lagunaires. *Messinian events in the Mediterranean*,
 618 7, 68-81.

619 Netzeband, G., Hübscher, C. & Gajewski, D. 2006. The structural evolution of the Messinian
 620 evaporites in the Levantine Basin. *Marine Geology*, 230, 249-273.

621 Ohneiser, C., Florindo, F., Stocchi, P., Roberts, A. P., Deconto, R. M. & Pollard, D. 2015. Antarctic
622 glacio-eustatic contributions to late Miocene Mediterranean desiccation and reflooding.
623 *Nature communications*, 6, 8765.

624 Ouillon, R., Lensky, N. G., Lyakhovsky, V., Arnon, A. & Meiburg, E. 2019. Halite precipitation from
625 double-diffusive salt fingers in the Dead Sea: Numerical simulations. *Water Resources*
626 *Research*, 55, 4252–4265. <https://doi.org/10.1029/2019WR024818>.

627 Pilcher, R. S. & Blumstein, R. D. 2007. Brine volume and salt dissolution rates in Orca Basin, northeast
628 Gulf of Mexico. *AAPG bulletin*, 91, 823-833.

629 Popescu, S.-M., Dalibard, M., Suc, J.-P., Barhoun, N., Melinte-Dobrinescu, M.-C., Bassetti, M. A.,
630 Deaconu, F., Head, M. J., Gorini, C. & Do Couto, D. 2015. Lago Mare episodes around the
631 Messinian–Zanclean boundary in the deep southwestern Mediterranean. *Marine and*
632 *Petroleum Geology*, 66, 55-70.

633 Roveri, M., Flecker, R., Krijgsman, W., Lofi, J., Lugli, S., Manzi, V., Sierro, F. J., Bertini, A., Camerlenghi,
634 A. & De Lange, G. 2014a. The Messinian Salinity Crisis: past and future of a great challenge
635 for marine sciences. *Marine Geology*, 352, 25-58.

636 Roveri, M., Lugli, S., Manzi, V., Gennari, R. & Schreiber, B. C. 2014b. High-resolution strontium
637 isotope stratigraphy of the Messinian deep Mediterranean basins: Implications for marginal
638 to central basins correlation. *Marine Geology*, 349, 113-125.

639 Ryan, W., Cita, M. & Hsü, H. 1973. The origin of the Mediterranean evaporates. *Initial Rep. Deep Sea*
640 *Drill. Proj*, 13, 1203-1231.

641 Ryan, W. B. 1973. Geodynamic implications of the Messinian crisis of salinity. *Messinian events in the*
642 *Mediterranean*. North-Holland Amsterdam.

643 Ryan, W. B. 1978. Messinian badlands on the southeastern margin of the Mediterranean Sea.
644 *Marine Geology*, 27, 349-363.

645 Ryan, W. B. 2009. Decoding the Mediterranean salinity crisis. *Sedimentology*, 56, 95-136.

- 646 Schmalz, R. F. 1991. The Mediterranean salinity crisis: Alternative hypotheses. *Carbonates and*
647 *evaporites*, 6, 121.
- 648 Simon, D. & Meijer, P. T. 2017. Salinity stratification of the Mediterranean Sea during the Messinian
649 crisis: A first model analysis. *Earth and Planetary Science Letters*, 479, 366-376.
- 650 Sirota, I., Arnon, A. & Lensky, N. G. 2016. Seasonal variations of halite saturation in the Dead Sea.
651 *Water Resources Research*, 52, 7151-7162.
- 652 Sirota, I., Enzel, Y. & Lensky, N. G. 2017. Temperature seasonality control on modern halite layers in
653 the Dead Sea: In situ observations. *GSA Bulletin*, 129, 1181-1194.
- 654 Sirota, I., Enzel, Y. & Lensky, N. G. 2018. Halite focusing and amplification of salt layer thickness:
655 From the Dead Sea to deep hypersaline basins. *Geology*, 46, 851-854.
- 656 Stern, M. E. 1960. The "salt-fountain" and thermohaline convection. *Tellus*, 12, 172-175.
- 657 Stiller, M., Gat, J. R. & Kaushansky, P. 1997. Halite precipitation and sediment deposition as
658 measured in sediment traps deployed in the Dead Sea: 1981-1983. *OXFORD MONOGRAPHS*
659 *ON GEOLOGY AND GEOPHYSICS*, 36, 171-183.
- 660 Stoica, M., Krijgsman, W., Fortuin, A. & Gliozzi, E. 2016. Paratethyan ostracods in the Spanish Lago-
661 Mare: More evidence for interbasinal exchange at high Mediterranean sea level.
662 *Palaeogeography, Palaeoclimatology, Palaeoecology*, 441, 854-870.
- 663 Van Simaey, S., Janszen, A., Hardy, C., Garnier, E., Sullivan, M., Fabuel-Perez, I., Spisto, Y. & Twigg, T.
664 Unravelling the Tectono-Stratigraphy of the Eratosthenes Continental Block. 81st EAGE
665 Conference and Exhibition 2019, 2019.
- 666 Vasiliev, I., Mezger, E. M., Lugli, S., Reichert, G.-J., Manzi, V. & Roveri, M. 2017. How dry was the
667 Mediterranean during the Messinian salinity crisis? *Palaeogeography, Palaeoclimatology,*
668 *Palaeoecology*, 471, 120-133.
- 669 Warren, J. 1999. *Evaporites: their evolution and economics*, Blackwell Science Oxford.

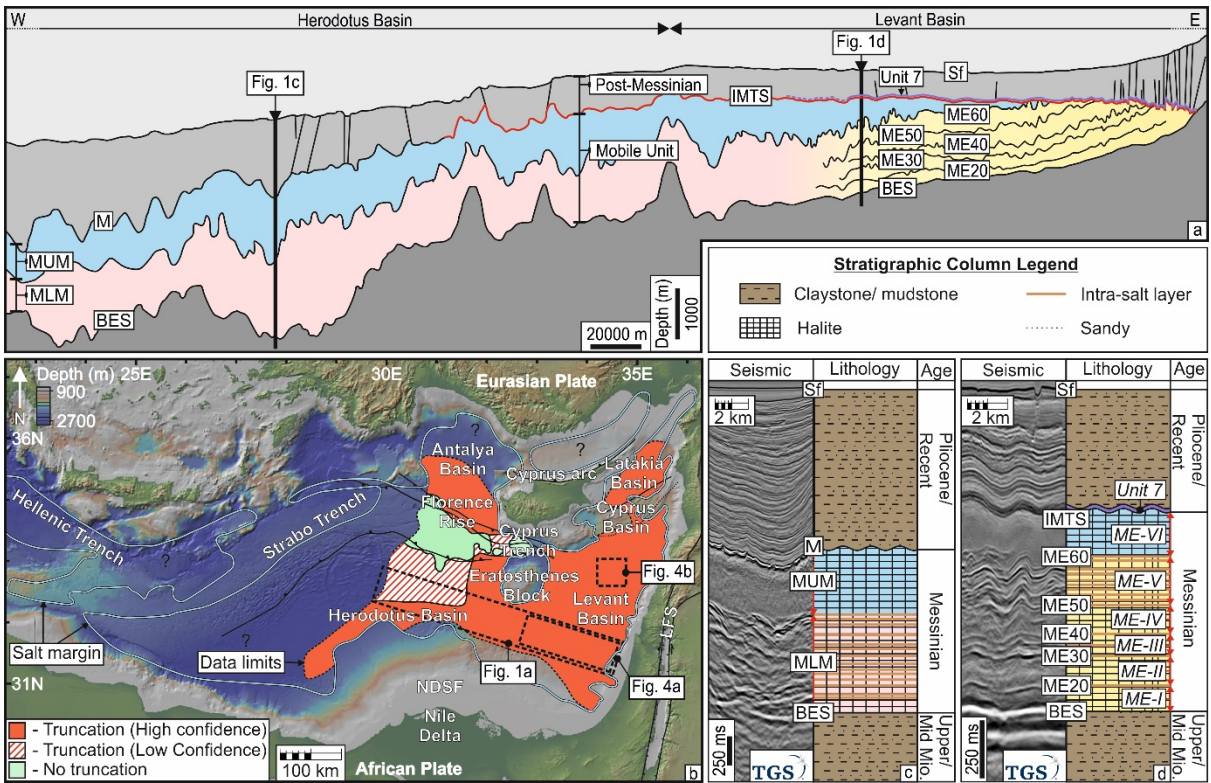


Figure 1. Regional truncation of the top of the Messinian salt sequence (Mobile Unit). **a:** E-W cross-section through the Herodotus Basin and Levant Basin showing the lateral variation in salt stratigraphy and geometry. **b:** Bathymetric map of the Eastern Mediterranean. The extent of the Messinian 'salt giant' is overlain (modified from (Lofi et al., 2011b)). Highlighted are regions where the top of the Mobile Unit has been truncated via dissolution (red & red striped) and where no truncation is observed (green). Blank areas within the salt margins (?) represent areas where seismic data quality is inadequate for this interpretation (northern Antalya Basin, Cyprus Arc and northern Latakia Basin) or there is no seismic data coverage (western Herodotus Basin and Hellenic Trench). NDSF – Nile deep sea fan; LFS – Levant fracture system. **c & d:** Seismic and lithological columns from the Herodotus Basin and Levant Basin respectively, demonstrating the contrasting stratigraphy within the Mobile Unit. IMTS – Intra-Messinian truncation surface; BES – Bottom erosional surface; Sf – Seafloor; M – Top salt; MUM – Messinian Upper Megasequence; MLM – Messinian Lower Megasequence.

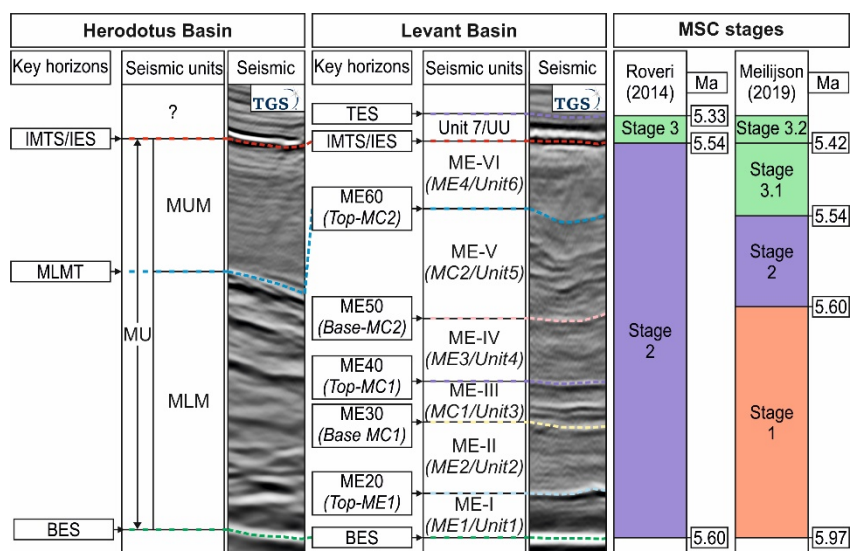


Figure 3. Seismic stratigraphy and chronostratigraphy of the Messinian evaporites in the Eastern Mediterranean. The main seismic units, key horizons and the various nomenclature (Bertoni and Cartwright, 2007; Lofi et al., 2011b; Feng et al., 2016; Gvirtzman et al., 2017; Lofi, 2018) for the Messinian evaporite sequence in the Levant Basin are outlined. These main seismic units are correlated with the two chronostratigraphic models of Roveri et al. (2014b) and Meilijson et al. (2019). IMTS – Intra-Messinian truncation surface; IES – Intermediate truncation surface; MUM – Messinian Upper Megasequence; MLM – Messinian Lower Megasequence; MLMT – Messinian Lower Megasequence Top; MU – Mobile Unit; BES – Bottom erosional surface; TES – Top erosional surface; UU – Upper Unit.

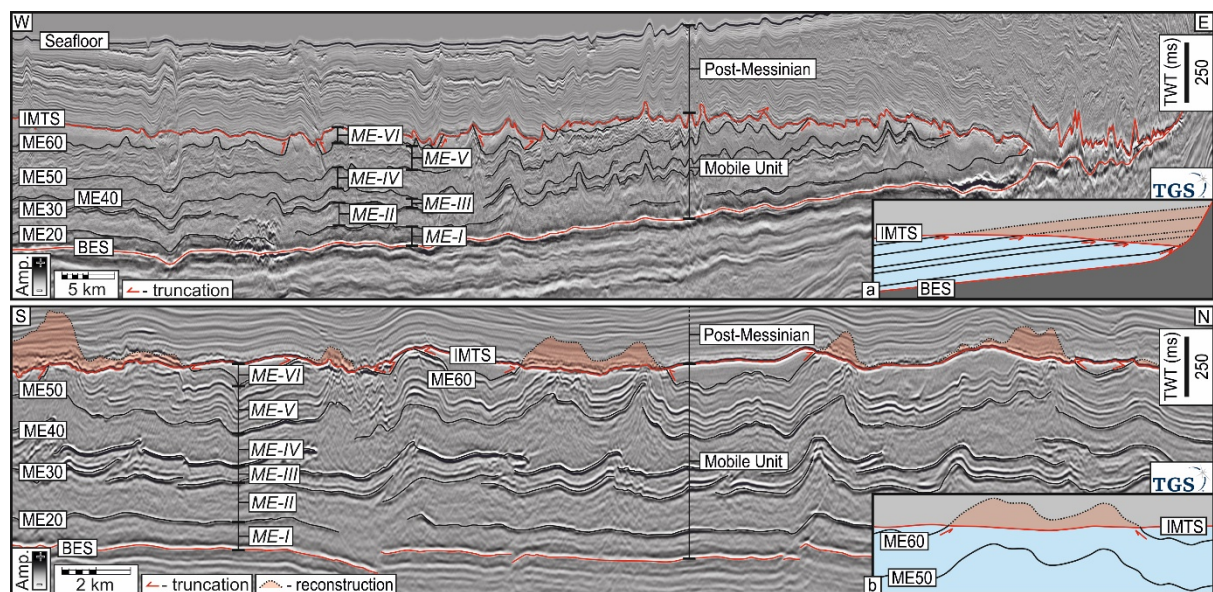


Figure 4. Marginal and abyssal truncation at the top of the Mobile Unit. Intra-Messinian deformation is evident where intra-salt layers at the top of the Mobile Unit are geometrically divergent to the IMTS (Intra-Messinian Truncation Surface) and the post-Messinian sequence. Intra-salt reflections are truncated by the IMTS. **a:** Marginal truncation of the Mobile Unit exhibited by subcropping intra-salt layers. The schematic projects a reconstruction of the intra-salt layers to the slope. **b:** Evidence for deep basin truncation where folded intra-salt layers are discordant with the IMTS (Intra-Messinian truncation surface). Where truncated, ME60 has been reconstructed. BES – Bottom erosional surface.

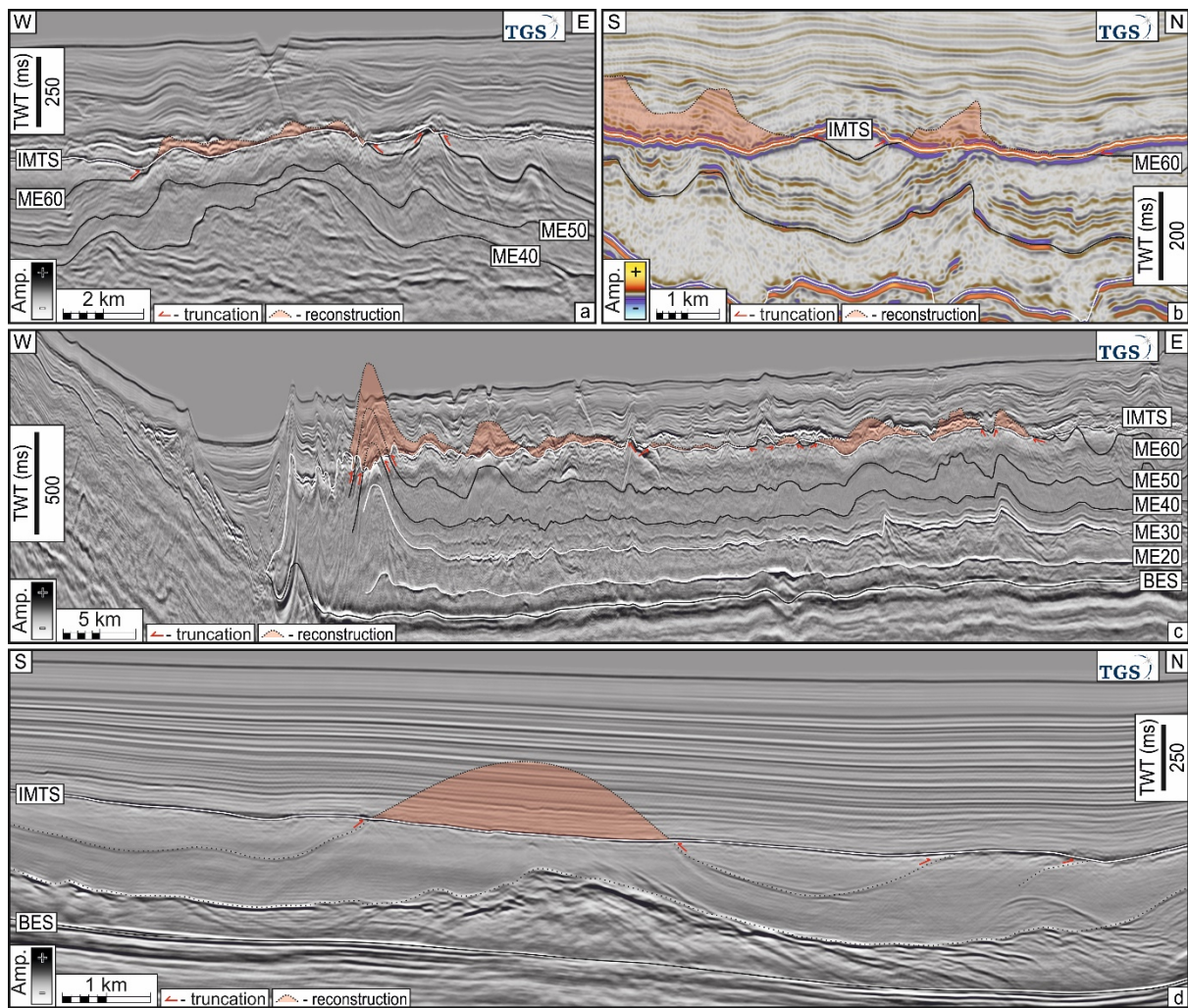


Figure 5. Examples of deformed intra-salt reflections that have been truncated from around the Eastern Mediterranean. Reconstructions of the truncated salt stratigraphy (red) demonstrate the significant amount and variability of vertically truncated stratigraphy around the basin. BES – Bottom Erosional Surface; IMTS – Intra-Messinian Truncation Surface. **a:** Truncation in the North Levant Basin. **b:** Truncation in the central Levant Basin. **c:** Truncation to the east of the Eratosthenes Block. **d:** Truncation in the Latakia Basin.

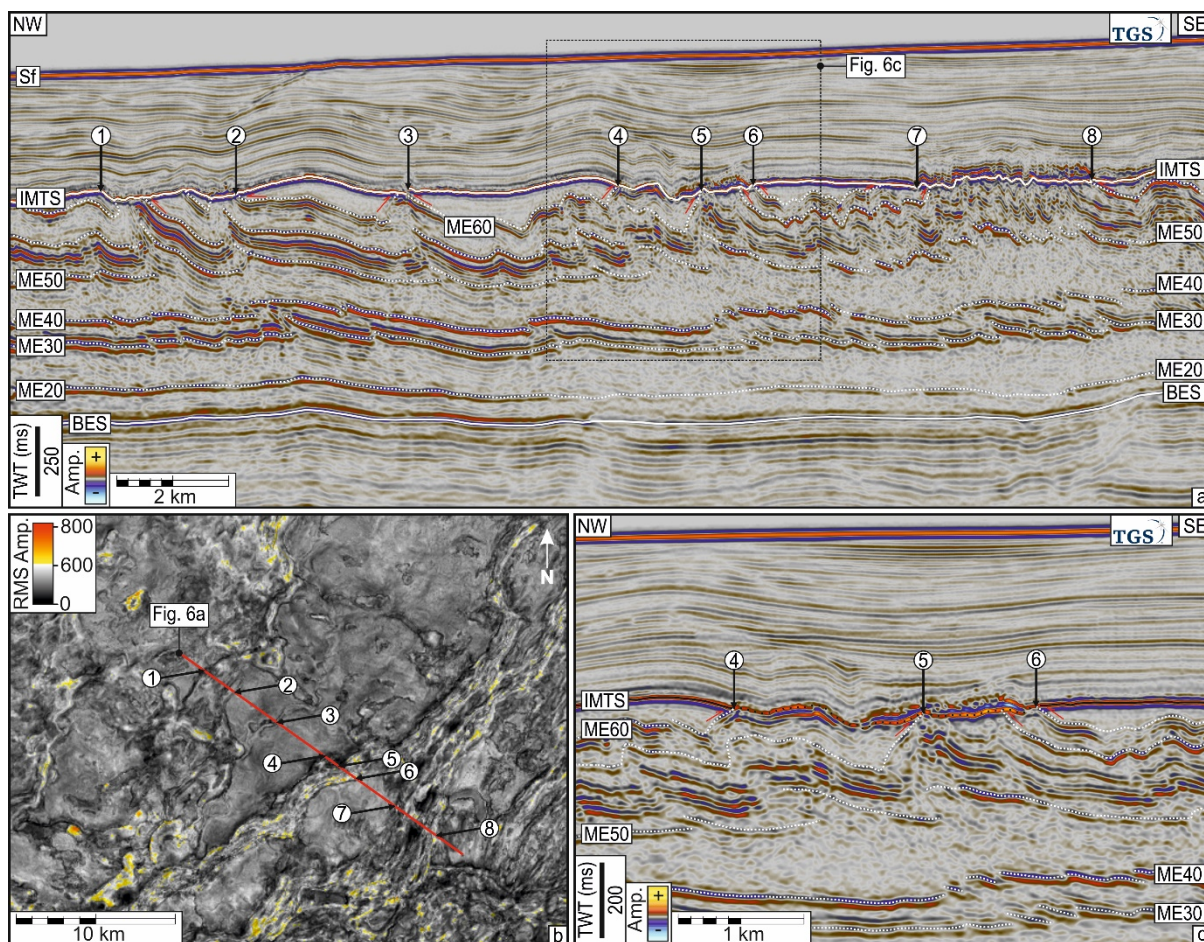


Figure 6. Local relict topography and increases in amplitude where intra-Messinian layers subcrop the intra-Messinian truncation surface (IMTS). **a:** A seismic cross-section from the 3D seismic survey offshore Lebanon (see Supplementary Fig. 1 for the location of the 3D survey) that displays several clear examples of intra-salt reflections that are truncated by the IMTS. Eight of these truncations have been highlighted (Numbers 1-8). **b:** An RMS amplitude map showing the locations of the eight truncations observed in Fig. 6a. The subcropping intra-Messinian reflections are exhibited as abrupt and linearly distributed increases in amplitude. **c:** A seismic cross-section showing a depression and rugose geometry of the IMTS at subcrops 4-6. BES – Bottom erosional surface.

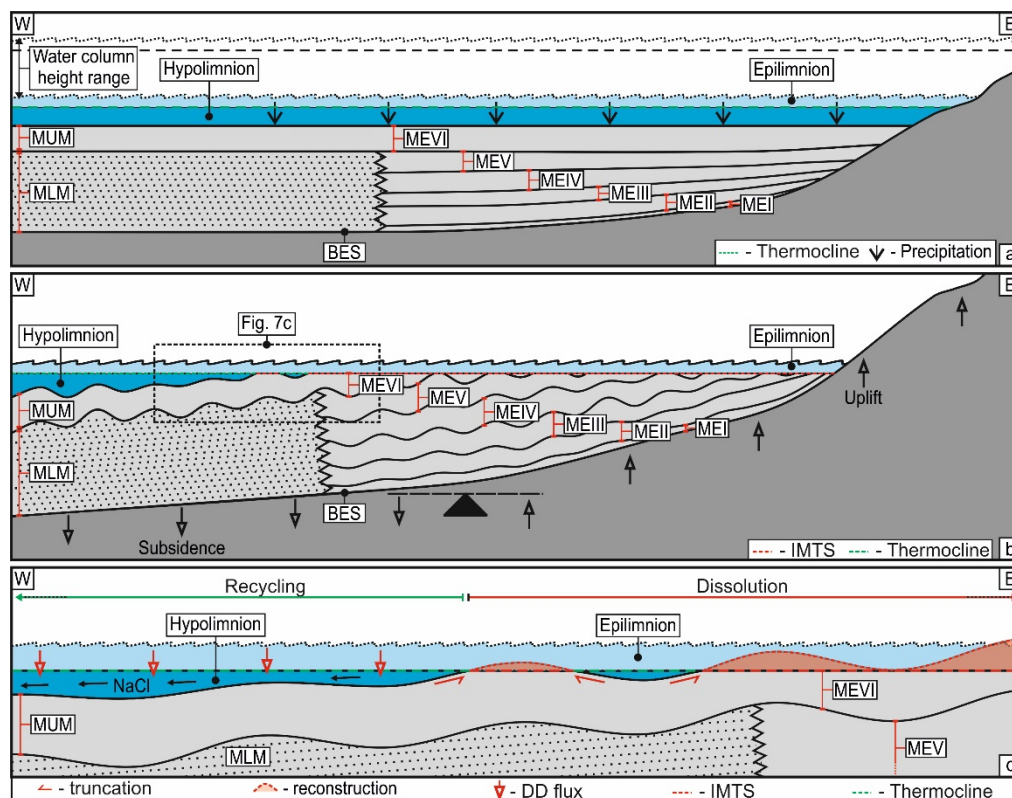


Figure 7. Model for uplift and thermal dissolution of salt in the Eastern Mediterranean. **a:** Deposition of salt sequence MEI-MEVI contemporaneous with deposition of the MLM (Messinian Lower Megasequence) and MUM (Messinian Upper Megasequence). **b:** Restriction at the Gibraltar Strait reduced seawater inflow into the basin, resulting in a relative sea level fall. Marginal uplift and subsidence drive late Messinian deformation of the salt. This uplifts the salt through the thermocline, resulting in dissolution within the epilimnion. **c:** Salt dissolved in the epilimnion is transferred to the hypolimnion via double diffusion (DD) salt fingering, where it can be recycled and re-precipitated at the hypolimnetic basin floor.